

Published in final edited form as:

*Lab Chip*. 2013 October 7; 13(19): 3903–3909. doi:10.1039/c3lc50540e.

## Electric Impedance Microflow Cytometry for Characterization of Cell Disease States†

E Du<sup>#a</sup>, Sungjae Ha<sup>#b</sup>, Monica Diez-Silva<sup>a</sup>, Ming Dao<sup>\*,a</sup>, Subra Suresh<sup>a</sup>, and Anantha P. Chandrakasan<sup>\*,b</sup>

<sup>a</sup>Department of Materials Science and Engineering, Massachusetts Institute of Technology, 77 Massachusetts Avenue, Cambridge, MA 02139, USA

<sup>b</sup>Department of Electrical Engineering and Computer Science, Massachusetts Institute of Technology, 77 Massachusetts Avenue, Cambridge, MA 02139, USA

# These authors contributed equally to this work.

### Abstract

The electrical properties of biological cells have connections to their pathological states. Here we present an electric impedance microflow cytometry (EIMC) platform for the characterization of disease states of single cells. This platform entails a microfluidic device for a label-free and non-invasive cell-counting assay through electric impedance sensing. We identified a dimensionless offset parameter  $\delta$  obtained as a linear combination of a normalized phase shift and a normalized magnitude shift in electric impedance to differentiate cells on the basis of their pathological states. This paper discusses a representative case study on red blood cells (RBCs) invaded by *Plasmodium falciparum* malaria parasites. Invasion of *P. falciparum* induces physical and biochemical changes on the host cells throughout a 48-h multi-stage life cycle within the RBC. As a consequence, it also induces progressive changes in electrical properties of the host cells. We demonstrate that the EIMC system in combination with data analysis involving the new offset parameter allows differentiation of *Pf*-invaded RBCs from uninfected RBCs as well as among different *P. falciparum* intraerythrocytic asexual stages including the ring stage. The representative results provided here also point to the potential of the proposed experimental and analysis platform as a valuable tool for non-invasive diagnostics of a wide variety of disease states and for cell separation.

### Introduction

Electric impedance spectroscopy (EIS) is a well established technique and has been widely utilized in the development of various biosensors.<sup>1</sup> This method offers a complementary technique for *in-vivo* detection of a variety of cancers including malignancy in the liver,<sup>2</sup> bladder,<sup>3</sup> skin<sup>4</sup> and breast.<sup>5</sup> For *in-vivo* EIS-based detection, the detectability and spatial resolution of lesions are highly limited by the contrast ratio of the focal region and its

†Electronic supplementary information (ESI) available.

© The Royal Society of Chemistry [year]

\*Corresponding authors: Ming Dao (mingdao@mit.edu) and Anantha P. Chandrakasan (anantha@mtl.mit.edu).

surroundings.<sup>6</sup> The electric impedance (EI) of the malignant tissues measured by EIS is relatively lower compared to those of normal tissues over radio frequency range.

Similarly, at the cellular level, variation in electrical properties of cells may be linked to the biochemical changes introduced by disease pathology. This variation can be detected through electrical impedance (EI) sensing of cell-substrate interactions, which was initiated by Giaever and Keese in 1984<sup>7</sup>. This method has been widely utilized to monitor cellular response to various stimuli, such as drug treatment,<sup>8</sup> infection by malaria parasite,<sup>9, 10</sup> and proliferation of leukaemia cells,<sup>11</sup> and to detect molecular or cell bounding events (through interactions of antibody-antigen, proteins, enzymes, etc.) such as those involving influenza virus<sup>12</sup> and breast cancer cells.<sup>13</sup> This method usually requires immobilization of a bio-recognition element on the surface of sensing electrodes or detection sites for enhanced specificity and signal amplification. Further recent developments include single-cell EI sensing systems utilizing microfluidic flow control in combination with microfabricated electrode structure,<sup>14-16</sup> which ensures high detection sensitivity as variations in electric current flow induced by the perturbation from cellular presence or biochemical interactions occur adjacent to sensing electrodes. Single-cell EI has been demonstrated to be an effective strategy for cell counting,<sup>17</sup> discrimination of various cell lines such as monocytes from dendritic cells and fibroblasts from adipocytes,<sup>18</sup> and detection of *Babesia bovis*-infected bovine red blood cells (RBCs).<sup>19</sup> Systematic modelling and simulation of the single-cell EI was conducted to link the dielectric properties to the cellular impedance response.<sup>20</sup> For parasitic diseases, EI sensing relies on the changes in electrical properties of cytoplasm and cell membrane, as the variation resulting from size changes of infected cells is negligible.

Diagnosis of malaria, an infectious disease threatening human health, relies on detection and counting of infected red blood cells (iRBCs). There were an estimated 216 million episodes of malaria and an estimated 655,000 malaria deaths in 2010, of which 91% were in Africa.<sup>21</sup> Among five types of *Plasmodium* infecting humans, *Plasmodium falciparum* is the deadliest strain causing malaria.<sup>22</sup> *P. falciparum* infection not only alters the membrane permeability of the host RBCs for nutrient uptake and waste disposal but also consumes hemoglobin of host RBCs forming hemozoin crystals.<sup>23</sup> Associated with these biochemical changes, the host RBCs undergo biophysical modifications of electrical,<sup>10</sup> optical,<sup>24</sup> mechanical,<sup>24, 25</sup> and magnetic<sup>26</sup> properties. The first application of EI measurement in physiological characterization for *P. falciparum* iRBCs (*Pf*-iRBCs) was performed using the cell-substrate interaction sensing.<sup>10</sup> The measurement was performed at the late intra-erythrocytic development stage. It also relied on a special method to trap RBCs based on antigen/antibody cross-linking and a self-assembled monolayer thus significantly limiting test throughputs. A recent work on single cell EI detection of mature stage *Pf*-iRBCs was realized based on conductance changes and characteristic dwell time using a graphene transistor integrated in a microfluidic channel.<sup>27</sup> The sensing was carried out in a “flow-catch-release” mode via bio-recognition protein functionalization on the graphene surface. Still, a high throughput (continuous flow detection) and high sensitivity diagnostic method for detecting *P. falciparum* infection, especially intraerythrocytic asexual ring stage, is necessary for field diagnostic tests and such a method is currently not available.

In this paper, we demonstrate an electric impedance microflow cytometry (EIMC) platform for reliable differentiation of each asexual maturation stage of *Pf*-iRBC. The EIMC platform is featured with continuous blood flow measurement without any cell immobilization treatment, target labelling, or electrode modification using bio-recognition elements. The performance of the EIMC system was tested with *Pf*-iRBCs. We considered both components of EI measurement of *Pf*-iRBCs, i.e. magnitude and phase, to establish a novel evaluation parameter for discrimination of different disease states.

## Materials and Methods

### *P. falciparum* Culture and Sample Preparation

*P. falciparum* was cultured in leukocyte-free human RBCs (Research Blood Components, Brighton, MA) under an atmosphere of 5% CO<sub>2</sub> balanced with N<sub>2</sub>, at 5% hematocrit in RPMI culture medium 1640 (Gibco Life Technologies) supplemented with 25 mM HEPES (Sigma), 200 mM hypoxanthine (Sigma), 0.20% NaHCO<sub>3</sub> (Sigma) and 0.25% Albumax II (Gibco Life Technologies). The cultured *P. falciparum* sample prior to EIMC measurement consisted of a mixture of multi-stage *Pf*-iRBCs and uninfected RBCs at parasitemia of 5% to 8%.

The working solution for EI measurement was phosphate-buffered saline (PBS; 2.67 mmol/l KCl, 1.47 mmol/l KH<sub>2</sub>PO<sub>4</sub>, 137.93 mmol/l NaCl, 8.06 mmol/l Na<sub>2</sub>HPO<sub>4</sub>·7H<sub>2</sub>O) mixed with Bovine Serum Albumin (BSA) (Sigma-Aldrich, St Louis, MO) to maintain osmotic pressure and prevent RBC adhesion to the microfluidic channel. Three concentrations of BSA-PBS, 0.2%, 0.5%, and 1% weight/volume (w/v) were utilized in the experiments to achieve optimum performance and sensitivity of EI measurement. The cultured *P. falciparum* samples were cooled down to room temperature after being removed from the incubator, then washed with PBS solution at 2000 rpm for 5 minutes at 21 °C and diluted by 200 times in the working solution.

### Microfluidic EIMC System

The experimental setup for EI measurement is shown in Fig. 1. The proposed microfluidic device for EI measurement consists of a microfluidic channel integrated with Ti/Au electrodes. The Ti/Au electrode of 10 nm/100 nm thickness was deposited on thin glass substrate (500 μm) using E-beam vaporization and standard microfabrication techniques. The microfluidic channel was fabricated using poly (dimethylsiloxane) PDMS casting protocols and bonded to the glass substrate. The two electrodes were 20 μm wide with 20 μm spacing embedded in the narrowest portion of the microfluidic channel (30 μm × 5 μm cross-sectional area) to probe individual human RBCs. The microfluidic EIMC system exhibited excellent optical qualities, allowing direct observation via microscopy. Measurements were performed on an Olympus IX 71 inverted microscope using a halogen source (100 W). Identification of *Pf*-iRBCs and specific stage was achieved using a long working distance lens with 100× magnification and numerical aperture NA = 0.8 (Olympus LMPLFLN100X). The electrodes were connected with an E4980A precision LCR meter (Agilent Technology, Inc.) for EI measurement. Communication between the LCR meter and data-recording computer was realized through a Keithley KUSB-488A USB-to-GPIB

cable. To reduce the error due to stray capacitance, the wires were connected in shielded two-terminal configuration. Lab-VIEW software (National Instruments Corp., Austin, TX) was used for automatic data acquisition.

The biochemical alterations during the multi-stage life cycle of *P. falciparum* lead to corresponding transitions in electrical properties of the host RBCs. As indicated by the equivalent circuit model of single *Pf*-iRBC suspended between two electrodes (see Supplementary Fig. S1(b), similar to the classic circuit model of single cells),<sup>1, 20</sup> the cell membrane capacitance shields the cell interior from the external electric field at low frequencies. At higher frequencies, owing to the short-circuiting effect of membrane capacitance, the electric field penetrates to the cellular interior and reaches the parasite. The present EI measurement was performed under a single frequency of 2 MHz with sampling rate of 50 Hz in order to probe both interfacial and intracellular changes of *Pf*-iRBCs. The frequency falls into the  $\beta$  dispersion regime (usually within the range of 0.1~10 MHz)<sup>28</sup> where the large discrepancy in conductivity of cellular membrane and cytoplasm causes a lag in charging response of the intracellular and extracellular substances. A continuous steady flow of evenly distributed cell suspension was generated by an exterior pressure gradient from two water columns, allowing minimum hydrodynamic disturbance during EI measurement while maintaining sufficient signal sampling. A stream of individual cell is managed where cells cross over electrodes with minimum bias from the midstream in order to maintain steady detection signal.

## Results

The proposed EIMC system possesses a cell-counting function. When a cell approaches and crosses the electrodes, the presence of the cell at the measuring zone forms a lossy capacitor, creating a dynamic impedance transition  $Z$  from the base impedance of the system. The EI transition is given by,

$$\Delta Z = Z_{s+Pf-iRBC} - Z_s \approx -Z_s^2 / (Z_s + Z_{Pf-iRBC}) \quad (1)$$

which is a complex function of cellular impedance  $Z_{Pf-iRBC}$  and medium impedance  $Z_s$  with the effects from the electric double layer (EDL) at the medium-electrode interfaces excluded (see Supplementary Fig. S1(c)). The magnitude deviation  $M$  and the phase deviation  $\phi$  are taken from the peaks of each  $Z$  transition, and they are complex functions of cell size, composition, dielectric properties of cytoplasm and the cell membrane, and the enclosure of the medium surrounding the cell.

Fig. 2 shows a typical example of EI transitions measured when cells cross the electrodes (see Supplementary Table S1 for EI transition statistics). Magnitude and phase changes,  $M$  and  $\phi$ , are shown in subplots. The insert in the phase change subplot displays a representative image for each sub-population, from uninfected RBCs to ring stage, trophozoite stage, and schizont stage.

In order to systematically evaluate different experimental conditions, EI transitions were normalized separately by,

$$x = \Delta\varphi / \overline{\Delta\varphi} \quad (2)$$

$$y = \Delta M / \overline{\Delta M} \quad (3)$$

where  $\overline{\Delta M}$  and  $\overline{\Delta\varphi}$  are the mean values of the magnitude change the phase change of 120 uninfected RBCs for the each corresponding BSA concentration (see Supplementary Table S1).

Detection of *P. falciparum* infection of RBCs was possible but limited based on either one of the normalized EI components in isolation. For 0.2% w/v BSA-PBS as demonstrated in Fig. 3, the normalized magnitude transition monotonically increases with the progressive malaria infection stages. The trend was not observed in normalized phase transition. Additionally, for higher BSA concentration conditions (0.5% w/v and 1% w/v), no consistent trends were found in either of the two normalized EI components as demonstrated in Supplementary Figs. S2 and S3. Fig. 3 shows statistically significant differences ( $P < 0.001$ ) in normalized EI magnitude between all three stages of *Pf*-iRBCs and uninfected RBCs, although no significant differences can be found between two adjacent *Pf*-iRBC stages.

In order to improve the disease state differentiation, we have established a new composite evaluation parameter to detect *Pf*-iRBCs at different stages. As Fig. 4(a) shows, the normalized EI components of uninfected RBCs at each BSA concentration can be well-fitted with linear curves as indicated by solid lines in the scatter plot. In Fig. 4(b), ring stage *Pf*-iRBCs are located in a slightly higher magnitude-phase region than the uninfected ones, and the late trophozoite and schizont *Pf*-iRBCs are obviously away from the other populations. In order to quantify this separation, we introduced a new dimensionless parameter, EI offset  $\delta$ , as the distance from each data point to the reference line,

$$\delta = - (kx_n + a - y_n) / \sqrt{k^2 + a^2} \quad (4)$$

where  $k$  and  $a$  are the linear interpolation coefficients of the normalized impedance transitions of uninfected RBCs;  $x_n$  and  $y_n$  are the normalized impedance transitions of individual RBCs. Although the normalized EI transitions varied between different experiments due to slight variations in sample and device preparation, a similar scatter pattern was observed. To combine data from each experiment, the scatter plots of EI transitions for *Pf*-iRBCs at various stages were aligned to have a common uninfected RBC reference line.

EI offsets  $\delta$  for various *Pf*-iRBC stages were compared to the uninfected RBCs using statistical box charts for different BSA concentrations, shown in Fig. 5. The statistical analysis was carried out using a two-sample t-test (see Supplementary Tables S2-S4). When BSA concentration was 0.2% w/v, all intraerythrocytic stages of *Pf*-iRBCs showed a statistically significant difference ( $P < 0.001$ ), as indicated in Fig. 5(a). With a small increase of BSA concentration to 0.5% w/v, all stages of *Pf*-iRBCs were still statistically different ( $P < 0.001$ ). When BSA concentration increases further to 1% w/v, the ring stage

bears moderate statistical significance ( $P = 0.134$ ) despite trophozoite and schizont stages still having high statistical significance ( $P < 0.001$ ). It is clear that the offset  $\delta$  is more scattered at higher BSA concentrations. In addition, the overlap between uninfected RBCs and *Pf*-iRBCs, especially for ring and trophozoite stages increases with BSA concentration. As shown in Fig. 5(a), we also found that, at 0.2% w/v, our new EI measurement method can be used to effectively distinguish *Pf*-iRBCs between adjacent asexual stages (trophozoite vs. ring, and schizont vs trophozoite) with high statistical significance.

## Discussion

One of the major challenges in non-invasive malaria diagnostics has been the lack of effective differentiation strategy of early stage *Pf*-iRBCs from uninfected RBCs. With the careful exploration of the optimum differentiation conditions, as shown in Fig. 3(a), using 0.2% w/v BSA-PBS, a statistically significant difference can now be found between ring stage *Pf*-iRBCs and uninfected RBCs, which had not been achieved in earlier studies using EI measurements.<sup>10, 27</sup>

We also recognized that BSA concentration may play an important role in separation of *Pf*-iRBCs from uninfected RBCs. *Pf*-iRBCs at mature stages (trophozoite and schizont) have elevated expression of membrane proteins [*Pf*EMP]-1, forming surface protrusions or “knobs,”<sup>29</sup> which bear a positive charge (+20 mV) as indicated by Surface Potential Spectroscopy.<sup>30</sup> The difference in the magnitude of EI transitions decreases with BSA concentration among various *Pf*-iRBC stages. This suggests that adsorption of negatively charged BSA<sup>31</sup> on the membrane of RBCs negates the surface charge modification associated with “knobs.” As a consequence, the inherent difference in surface charge density between different *Pf*-iRBC stages is likely to be minimized. This finding suggests that the lowest BSA concentration we tested, 0.2% w/v, was an optimum condition of the present EIMC system for *P. falciparum* diagnostic purposes while maintaining continuous flow of cells. Lower BSA concentration than 0.2% w/v may result in adhesion of cells to the channel walls and consequently ineffective or even impossible EI data collection.

Using the new parameter, EI offset  $\delta$ , we have demonstrated significantly improved resolution and effectiveness in the detection of *Pf*-iRBCs and among various intraerythrocytic asexual stages using single frequency excitation. The consistent linear interpolation between the normalized magnitude and phase transitions of uninfected RBCs establishes a reliable base line. This reference line is carefully chosen to be the mean trend of the measurements from uninfected cells; however, it can be the mean trend from entire population at field diagnostic applications since uninfected RBC population is always dominant (> 90%), even in severe malaria cases.<sup>32</sup>

Studies of cell impedance had enabled a possible label-free diagnostic test by recourse to the measurement of specific parameters.<sup>33</sup> However, systematic demonstration of the evolution of cell pathological states has thus far not been reported. Indeed, accurate measurements of biophysical properties of a cell in a microfluidic device is usually limited by such factors as the high impedance of probe electrodes, stray capacitance, and electric double layer capacitance. In addition, the presence of the intra-erythrocytic parasite also alters the

progressive evolution of the electric response of the cell. In light of these issues, well-controlled and systematic experiments linking cell electrical response from healthy to early disease states to fully pathological states have thus far not been fully successful.

In this paper, we have overcome these limitations by establishing a new parameter, EI offset  $\delta$ , which contains both magnitude and phase information of the entire cell suspended in the medium. This parameter appears to provide a promising new marker for identifying the onset and progression of disease states at the cell level. By properly accounting for both EI magnitude and phase information, the single offset parameter enables the identification of progressive changes in the pathological state of a red blood cell invaded by the parasite. The improved detectability of the subtle differences between disease states (e.g. *P. falciparum* ring stage iRBCs versus uninfected RBCs) suggests that the EIMC system presented in this study may be adapted for improving disease state differentiation of different cell populations and other disease classes involving electrical property changes. Sickle cell anemia and acidosis are among the diseases that are likely to have changes in EI properties of RBCs, and would be interesting topics of future systematic studies. By using the changes in electrical signature to identify the evolution of cell disease states, the present method provides an additional tool to recent advances whereby changes in mechanical signature<sup>34, 35</sup> or membrane flickering<sup>24</sup> have been linked as markers to detect cell disease states. To advance the state of the art and overcome any remaining limitations, more systematic efforts need to be carried out for practical medical applications.

## Conclusion

The proposed microfluidic EIMC system provides a non-invasive and reliable detection method for *P. falciparum* infection. The detection of *P. falciparum* ring stage iRBCs in 0.2% BSA-PBS medium was achieved using normalized EI magnitude. Furthermore, with a newly developed dimensionless parameter, EI offset  $\delta$ , the ring-stage *Pf*-iRBC detection was significantly improved. Statistically significant differentiation of *Pf*-iRBCs was also achieved between adjacent intraerythrocytic maturation stages (trophozoite vs. ring, and schizont vs trophozoite). The sensitivity of the *Pf*-iRBC detection and EIMC performance were found to be significantly influenced by BSA concentration and a number of other relevant factors, such as cell concentration, flow rate, sampling rate. The results indicate that 0.2% w/v BSA in PBS is optimum for the present EIMC measurement with sufficient detection sensitivity while minimizing cell adhesion to microfluidic channel. The newly developed method using the composite parameter  $\delta$ , instead of the single EI component approach in an approximated circuit model, is also expected to be more broadly applicable in differentiating other types of diseased cells for disease diagnostics and cell separation.

## Supplementary Material

Refer to Web version on PubMed Central for supplementary material.

## Acknowledgments

Sungjae Ha acknowledges Fulbright Science and Technology Award. We thank S. J. Kim and J. Han for help in the initial system development and discussion in background experimental work. Device fabrications were carried out

at MIT Microsystems Technology Laboratories. The authors acknowledge support by the National Research Foundation (Singapore) through Singapore-MIT Alliance for Research and Technology (SMART) Center (ID IRG), MIT Center for Integrated Circuits and Systems (CICS), and the U. S. National Institutes of Health (Grant R01 HL094270).

## References

1. Pethig R, Kell DB. *Phys Med Biol.* 1987; 32:933–970. [PubMed: 3306721]
2. O'Rourke AP, Lazebnik M, Bertram JM, Converse MC, Hagness SC, Webster JG, Mahvi DM. *Phys Med Biol.* 2007; 52:4707–4719. [PubMed: 17634659]
3. Keshtkar A, Keshtkar A, Smallwood RH. *Physiol Meas.* 2006; 27:585–596. [PubMed: 16705257]
4. Glickman YA, Filo O, David M, Yayon A, Topaz M, Zamir B, Ginzburg A, Rozenman D, Kenan G. *Skin Res Technol.* 2003; 9:262–268. [PubMed: 12877689]
5. Malich A, Bohm T, Facius M, Kleinteich I, Fleck M, Sauner D, Anderson R, Kaiser WA. *Nucl Instrum Meth A.* 2003; 497:75–81.
6. Malich A, Facius M, Anderson R, Bottcher J, Sauner D, Hansch A, Marx C, Petrovitch A, Pfeleiderer S, Kaiser W. *Eur Radiol.* 2003; 13:2441–2446. [PubMed: 12845465]
7. Giaever I, Keese CR. *Proc Natl Acad Sci-Biol.* 1984; 81:3761–3764.
8. Asphahani F, Wang K, Thein M, Veisoh O, Yung S, Xu JA, Zhang MQ. *Phys Biol.* 2011; 8
9. Tripathi AK, Sullivan DJ, Stins MF. *J Infect Dis.* 2007; 195:942–950. [PubMed: 17330783]
10. Ribaut C, Reybier K, Reynes O, Launay J, Valentin A, Fabre PL, Nepveu F. *Biosens Bioelectron.* 2009; 24:2721–2725. [PubMed: 19167879]
11. Hao C, Yan F, Ding L, Xue YD, Ju HX. *Electrochem Commun.* 2007; 9:1359–1364.
12. Meseko CA, Oladokun AT, Ekong PS, Fasina FO, Shittu IA, Sulaiman LK, Egbuji AN, Solomon P, Ularamu HG, Joannis TM. *Diagn Micr Infec Dis.* 2010; 68:163–165.
13. Srinivasaraghavan V, Strobl J, Agah M. *Lab Chip.* 2012; 12:5168–5179. [PubMed: 23108380]
14. Ayliffe HE, Frazier AB, Rabbitt RD. *J Microelectromech S.* 1999; 8:50–57.
15. Malleo D, Nevill JT, Lee LP, Morgan H. *Microfluid Nanofluid.* 2010; 9:191–198. [PubMed: 20927185]
16. Wang MH, Kao MF, Jang LS. *Rev Sci Instrum.* 2011; 82
17. Sohn LL, Saleh OA, Facer GR, Beavis AJ, Allan RS, Notterman DA. *Proc Natl Acad Sci USA.* 2000; 97:10687–10690. [PubMed: 10995481]
18. Schade-Kampmann G, Huwiler A, Hebeisen M, Hessler T, Di Berardino M. *Cell Proliferat.* 2008; 41:830–840.
19. Valero A, Braschler T, Renaud P. *Lab Chip.* 2010; 10:2216–2225. [PubMed: 20664865]
20. Morgan H, Sun T, Holmes D, Gawad S, Green NG. *J Phys D: Appl Phys.* 2007; 40:61–70.
21. World Malaria Report 2010. World Health Organization; Geneva: 2010. p. 1-204.
22. Dondorp AM, Pongponratn E, White NJ. *Acta Trop.* 2004; 89:309–317. [PubMed: 14744557]
23. Sherman IW. *Microbiol Rev.* 1979; 43:453–495. [PubMed: 94424]
24. Park YK, Diez-Silva M, Popescu G, Lykotrafitis G, Choi WS, Feld MS, Suresh S. *Proc Natl Acad Sci USA.* 2008; 105:13730–13735. [PubMed: 18772382]
25. Bow H, Pivkin IV, Diez-Silva M, Goldfless SJ, Dao M, Niles JC, Suresh S, Han JY. *Lab Chip.* 2011; 11:1065–1073. [PubMed: 21293801]
26. Hackett S, Hamzah J, Davis TME, St Pierre TG. *Bba-Mol Basis Dis.* 2009; 1792:93–99.
27. Ang PK, Li A, Jaiswal M, Wang Y, Hou HW, Thong JTL, Lim CT, Loh KP. *Nano Lett.* 2011; 11:5240–5246. [PubMed: 22077950]
28. Schwan HP. *Med Prog Technol.* 1993; 19:163–165. [PubMed: 8052170]
29. Aikawa M, Kamanura K, Shiraishi S, Matsumoto Y, Arwati H, Torii M, Ito Y, Takeuchi T, Tandler B. *Exp Parasitol.* 1996; 84:339–343. [PubMed: 8948323]
30. Gruenberg J, Allred DR, Sherman IW. *J Cell Biol.* 1983; 97:795–802. [PubMed: 6350320]
31. Bohme U, Scheler U. *Chem Phys Lett.* 2007; 435:342–345.
32. Hanscheid T. *Clin Lab Haematol.* 1999; 21:235–245. [PubMed: 10583325]

33. Sun T, Morgan H. *Microfluid Nanofluid*. 2010; 8:423–443.
34. Suresh S. *Acta Biomater*. 2007; 3:413–438. [PubMed: 17540628]
35. Suresh S, Spatz J, Mills JP, Micoulet A, Dao M, Lim CT, Beil M, Seufferlein T. *Acta Biomater*. 2005; 1:15–30. [PubMed: 16701777]



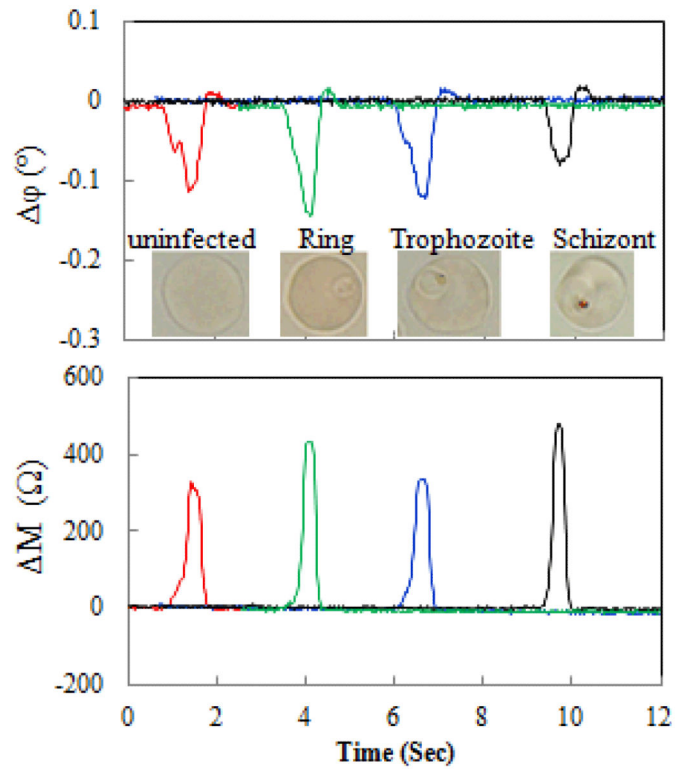


**Fig.2.** EI transitions measured as uninfected RBCs and Pf-iRBCs crossed over the electrode probe. Measurement conditions: 2MHz 1V and 0.2% w/v BSA-PBS.

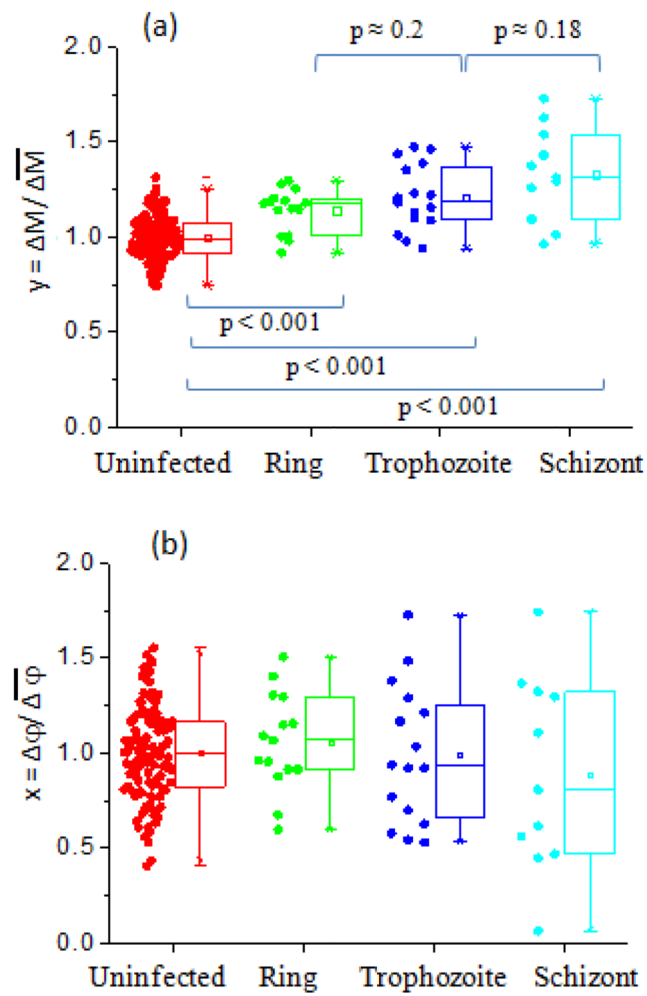


**Fig. 3.** (a) Scatter plot of normalized magnitude transition for uninfected RBCs and *Pf*-iRBCs in 0.2% w/v BSA-PBS. (b) Scatter plot of normalized phase transition for uninfected RBCs and *Pf*-iRBCs in 0.2% w/v BSA-PBS.

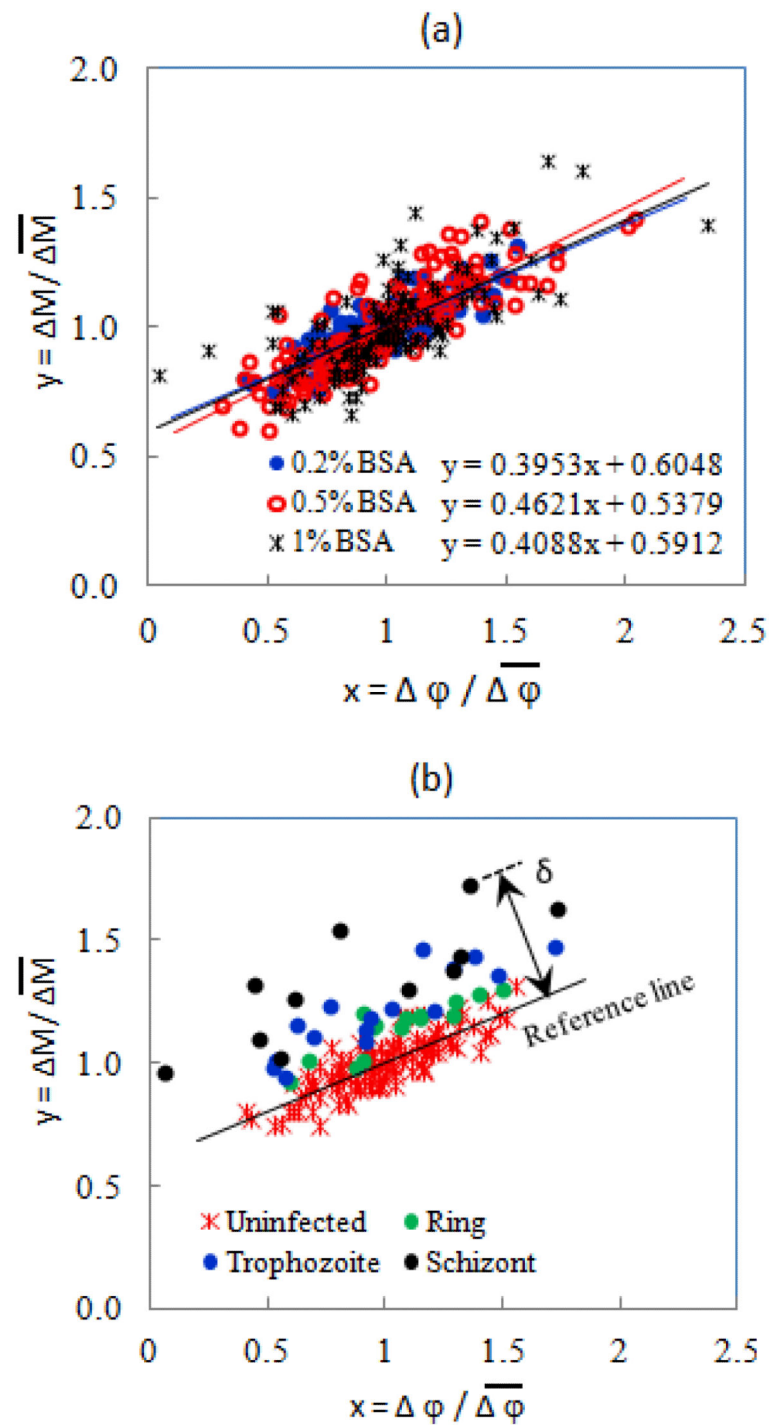


**Fig. 4.** (a) Scatter plot of normalized EI transitions of uninfected RBCs. (b) Scatter plot of normalized EI transitions for 0.2% BSA-PBS and definition of Offset  $\delta$ .

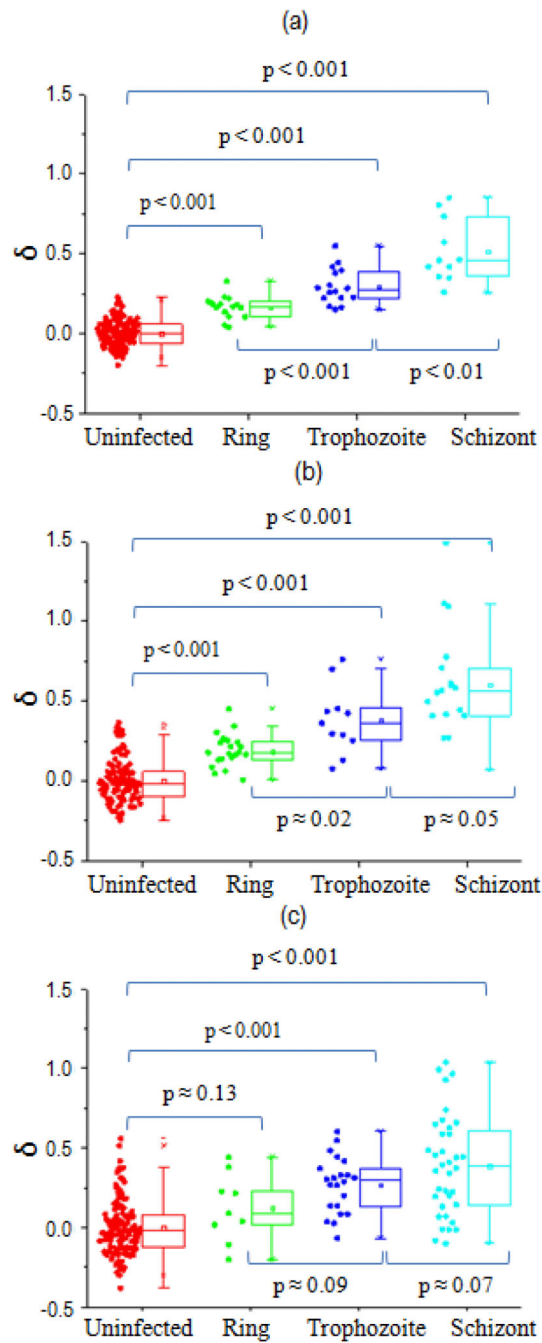


**Fig. 5.** *Pf*-iRBC separation results in (a) 0.2% w/v BSA-PBS, (b) 0.5% w/v BSA-PBS, and (c) 1% w/v BSA-PBS.